Green Chemical Technology

SCIEPublish

Article

Optimization of Fly Ash-Based Composite Cementitious Material Proportion Using Box-Behnken Response Surface Methodology

Haoyu Xia [1], Liu Zhang [1], Ziyu Zou [1], Zecheng Zeng [1], Mengqi Zeng [1], Zhenjun Wu [1,*] and Xiuqiang Xie [2,*]

[1] College of Chemistry and Chemical Engineering, Hunan University, Changsha 410082 China; haoyuxia@hnu.edu.cn (H.X.); chris022@hnu.edu.cn (L.Z.); ZouZiyu@hnu.edu.cn (Z.Z.); z235011@hnu.edu.cn (Z.Z.); zmq123321@hnu.edu.cn (M.Z.)

[2] College of Materials Science and Engineering, Hunan University, Changsha 410082, China

* Corresponding author. E-mail: wooawt@hnu.edu.cn (Z.W.); xiuqiang_xie@hnu.edu.cn (X.X.)

Received: 23 January 2026; Revised: 2 March 2026; Accepted: 31 March 2026; Available online: 9 April 2026

ABSTRACT: To realize high-value synergistic utilization of the three major solid wastes from thermal power generation (fly ash-FA, coal-fired slag-CS, desulfurization gypsum-DG), a Box-Behnken response surface model was established with CS, DG, and cement as factors and FA as the matrix. Unlike existing research focusing on single or binary solid waste composites, this study systematically optimized the synergistic blending ratios of the three wastes without additional activation. The 7d/28d strength models showed significant statistical validity (R^2 = 0.9918/0.9979, $p < 0.001$). The optimal mix ratio (CS 21.38%, DG 10.96%, cement 16.15%, FA 51.51%) achieved 7d strength of 13.60 MPa and 28d strength of 19.07 MPa, with a model deviation rate below 2%. The statistical model results are deeply correlated with the mechanisms of hydration and microstructural evolution: cement and DG drive early-stage hydration reactions to form rapid-strength products, while CS continuously generates hydration gel through slow pozzolanic reactions to develop late-stage strength. XRD/SEM analysis confirmed significant formation of calcium-aluminum-silicate hydrate (C-(A)-S-H), calcium hydroxide (CH), and ettringite (AFt), verifying full activation of pozzolanic substances in FA and CS. This study innovatively overcomes bottlenecks in the simultaneous high-value utilization of three thermal wastes, providing a scientific pathway for optimizing cementitious materials from multi-source solid wastes.

Keywords: Response surface methodology; Fly ash; Coal-fired slag; Desulfurization gypsum; Composite cementitious material

1. Introduction

As China's society transitions from high-speed development to high-quality development and urbanization continues to advance, the total energy consumption continues to grow. Thermal power generation remains the dominant form of electricity supply in China. As of September 2025, the nation's cumulative installed power generation capacity reached 3.72 billion kilowatts. Thermal power accounted for 1.53 billion kilowatts, about 40.4 per cent of the total. Thermal power generation, while ensuring energy

security, produces substantial quantities of fly ash (FA), coal-fired slag (CS), and desulfurization gypsum (DG), collectively known as the three major solid wastes of thermal power generation. According to data from China's National Bureau of Statistics, solid waste production from thermal power generation has shown an upward trend over the past decade. By 2024, FA output exceeded 700 million tons. The total of the three major solid wastes from thermal power generation surpassed 900 million tons. For a considerable period, solid waste from thermal power generation has predominantly relied on extensive management approaches such as open-air stockpiling or rudimentary landfill disposal. These problems have become the core bottleneck restricting the green transformation of China's thermal power sector [1]. In response to this grave situation, China has introduced a number of policies and measures, through a series of guiding documents, including the Circular Economy Development Plan for the 14th Five-Year Plan Period and the Implementation Opinions on Accelerating the Comprehensive Utilization of Industrial Resources, clear arrangements have been made regarding the scale and technological depth of resource recovery for bulk solid wastes such as FA, CS, and DG. Driven by the Key Work Plan for Comprehensive Utilization of Bulk Solid Waste jointly issued by multiple ministries in 2021, the thermal power solid waste disposal sector is gradually moving from low-value disposal to high-value synergistic utilization.

Despite the gradual emergence of policy leverage effects, deep-seated contradictions in the resource utilization of solid waste from thermal power generation persist, and the overall level of development still holds considerable room for improvement [2]. More importantly, under the dual carbon strategy waste materials toal carbon strategy, the functional positioning of resource utilization for industrial solid wastes has changed fundamentally. It has shifted from mere end-of-pipe pollution control to source-based carbon reduction and mitigation. From a life cycle assessment (LCA) perspective [3], solid waste from thermal power generation exhibits a notably low carbon content. Notably, ordinary Portland cement (OPC) production is a major source of carbon emissions, accounting for approximately 5–10% of global anthropogenic CO_2 emissions. Concrete is the most widely used construction material. Its massive consumption leads to huge OPC demand, further worsening the carbon footprint of the construction industry [4,5]. Therefore, the use of waste materials to replace traditional high-energy-consuming cement clinker in constructing a low-carbon cement system is the core approach to reducing carbon emissions intensity in the building materials industry [6,7]. Relevant research has confirmed the feasibility of thermal power solid waste as a raw material for cementitious materials and initially explored the activation effect of single or double solid waste compounding: Xu et al. [8], developed a novel composite cementitious material for mine backfilling by partially substituting cement clinker with DG and CS. This innovation achieves significant carbon reduction while meeting practical application requirements. Ruan et al. [9], employed DG to activate magnesium slag and FA cement paste backfill material. Their research revealed that the incorporation of DG not only enhanced the system's strength but also improved its durability. Microscopic analysis showed that DG promoted hydration reactions, accelerating the formation of AFt and C-(A)-S-H. Additionally, researchers have verified that the active silica-alumina components (SiO_2, Al_2O_3) can undergo depolymerization-polycondensation reactions in an alkaline-activated environment to generate C-(A)-S-H gels and other hydration products, endowing the material with cementitious hardening properties [10–12]. Researchers have utilized waste materials or natural resources such as sludge (including industrial sludge, municipal sludge, and marine sludge), natural sea sand, coral sand, and river sand to develop low-carbon composite cementitious materials through multi-response approaches. This strategy has been proven to be an effective solution for addressing bulk solid waste and reducing carbon emissions in cement production [13–16]. More notably, existing research has demonstrated that high-fly-ash-content composites exhibit enhanced durability through intrinsic self-healing mechanisms. This is crucial for extending the long-term service life of cementitious materials [17,18]. These findings indicate that fly-ash-based composites not only promote sustainable development through the resource utilization of solid waste but also possess inherent self-healing potential. They can mitigate microcracks and improve long-term

durability. These studies lay a theoretical and experimental foundation for the utilization of thermal power solid waste in cementitious materials, and also confirm the potential of synergistic activation of multiple solid wastes to improve material performance.

However, the majority of existing research still has obvious limitations in methodological design, synergistic mixing of multiple wastes, and comprehensive high-value utilization of thermal power solid waste. It mainly adopts a single-factor variable approach or simple binary compounding, blending thermal power solid waste with other materials to produce cementitious materials, mine backfill, or concrete. This method fails to quantify the non-linear interaction between multiple solid waste components, and neglects the systematic synergistic disposal and proportion optimization for the three major categories of thermal power solid waste (FA, CS, DG), resulting in the accumulation and difficult treatment of certain thermal power solid wastes. Besides, similar to the regional variations in sludge characteristics highlighted in relevant reviews [13], fly ash, bottom ash, and coal ash from different regions in China also exhibit distinct geographical distribution patterns. This is due to regional differences in coal quality, combustion technology, and desulfurization processes. For example, fly ash from southern plants has higher CaO and moisture content. Coastal fly ash often contains elevated chloride ions due to maritime coal transportation. Inland plant bottom ash may have higher sulfate purity because of stricter desulfurization controls. Particularly in high-ash production areas and western thermal power bases, FA output is substantial yet of inconsistent quality. There is a lack of targeted proportion schemes to realize the simultaneous and high-value utilization of FA, CS, and DG. This makes it impossible to achieve simultaneous utilization of the three wastes, leading to massive waste accumulation and severe inventory backlogs over time [19]. Furthermore, constrained by the complexity and diversity of the physicochemical properties of solid waste feedstocks, such as low inherent reactivity, significant compositional fluctuations, and impurity enrichment. Cementitious materials prepared by simple compounding of multiple solid wastes (without scientific proportion optimization) often have problems such as low early-stage strength and poor durability. Additional modifications, such as chemical activation or high-temperature treatment, are required to regulate these properties [20]. This increases application costs and limits large-scale industrial promotion. The aforementioned issues present unprecedented challenges for the synergistic disposal of the three major solid wastes from thermal power generation. Thus, there is an urgent need to adopt a scientific multi-factor optimization method to regulate the solid waste ratio and fully activate material properties. This approach must simultaneously facilitate the synergistic disposal of these three major thermal power wastes while meeting the requirements of engineering applications.

Against this backdrop, this study breaks through the core limitations of existing research and achieves multiple innovative explorations in the high-value synergistic utilization of thermal power solid wastes and the proportional optimization of composite cementitious materials. The study proposes using the Box-Behnken response surface design (BBD) to construct a three-factor multi-material synergistic model and optimize the composition of composite cementitious materials. The use of machine learning algorithms to study the mix design optimization of composite cementitious materials has been proven to significantly enhance optimization capabilities [21–25]. In this study, BBD visualization technology was employed to comprehensively analyze the main effects of individual factors and their non-linear interactions. This enables rapid identification of optimal formulations while balancing experimental efficiency with optimization precision. Distinct from existing studies that focus on binary solid waste compounding or single-factor exploration [26], this work takes low-reactivity FA—the most produced and difficult-to-utilize core solid waste in thermal power generation—as the matrix, and systematically couples CS and DG as dual activators with a small amount of cement as an alkaline regulator. It for the first time constructs a composite cementitious system based on the synergistic utilization of the three major thermal power solid wastes, without additional chemical activation or high-temperature modification treatment. The objective is to develop a novel cementitious material capable of fully activating the properties of multiple solid wastes

while performing well in the later-stage strength without additional chemical activation or high-temperature treatment. Moreover, this research innovatively combines macroscopic mechanical property tests with XRD and SEM microscopic characterization techniques. It deeply reveals the differential regulation effects of the three major thermal power solid wastes on the early and late-stage strength of the composite system. It also clarifies the internal micro-mechanism of the synergistic activation of low-reactivity FA by CS and DG. This is a key supplement to the existing research on the hydration mechanism of solid waste-based cementitious materials. This work not only provides a scientific and efficient methodological reference for the proportion optimization of multi-solid waste composite cementitious materials. It also opens up a new technical route for the large-scale high-value synergistic utilization of the three major thermal power solid wastes. In addition, it lays a solid experimental and theoretical foundation for the green and low-carbon transformation of the building materials industry.

2. Materials and Methods

2.1. Materials

The raw materials for this experiment comprised FA, CS, DG, and cement. The three major solid wastes from thermal power generation were sourced from a power plant in Guizhou Province, whilst the cement was P·O 42.5 grade cement produced by Beijing Cement Group Jidong (Beijing, China). The chemical composition of each raw material is shown in Table 1, XRD analysis is presented in Figure 1, and the macroscopic morphology of FA, CS, DG, and Cement is depicted in Figure 2. The raw materials were ground in a cement ball mill for 30 min, then passed through a 0.074 mm screen. The laser particle size analysis results are shown in Figure 3. FA is a reddish-brown powder with a relatively fine particle size, produced by incomplete calcination at 400–600 °C and containing significant impurities such as hematite and olivine. CS also exhibits a powdery form, with an overall particle size slightly larger than FA. Its particles are irregular in shape, possessing a relatively loose texture and a coarse surface. It is greyish-brown and exhibits characteristic structural features indicative of high-temperature melting and subsequent cooling. CS is rich in CaO (44.20%) and silicate components, which are the material basis for its slow pozzolanic reaction in the later hydration stage to generate C-S-H gel. DG has a moisture content of approximately 25%, exhibiting a macroscopic morphology characterized by the coexistence of powdery and lumpy phases. The powdery fraction is fine and uniform, while the lumpy fraction predominantly consists of irregular agglomerates, appears pale yellow. It has a high SO_3 content (51.98%), which can provide a large amount of SO_4^{2-} for the rapid formation of AFt crystals in the early hydration stage. This fluctuation in moisture content constitutes a significant limitation of this study, as highlighted by the reproducibility challenges noted in related research [13]—moisture variation affects the actual effective dosage of DG, alters the water-cement ratio of the system, and consequently impacts the uniformity of hydration reactions and the consistency of mechanical properties. To mitigate this issue, DG was pre-weighed prior to use and homogenized by air-drying to a constant weight.

Table 1. Chemical composition analysis of raw materials.

Material	MgO	Al_2O_3	SiO_2	SO_3	CaO	TiO_2	Fe_2O_3	Loss
Fly ash	0.92	19.65	29.88	11.39	15.44	2.81	16.53	3.392
Coal-fired slag	0.74	7.49	10.81	24.56	44.20	1.66	9.02	1.5249
Desulfurization gypsum	0.62	0.62	1.31	51.98	44.68	0.08	0.37	0.3471
Cement	1.14	5.22	22.24	0.52	65.73	-	3.77	1.38

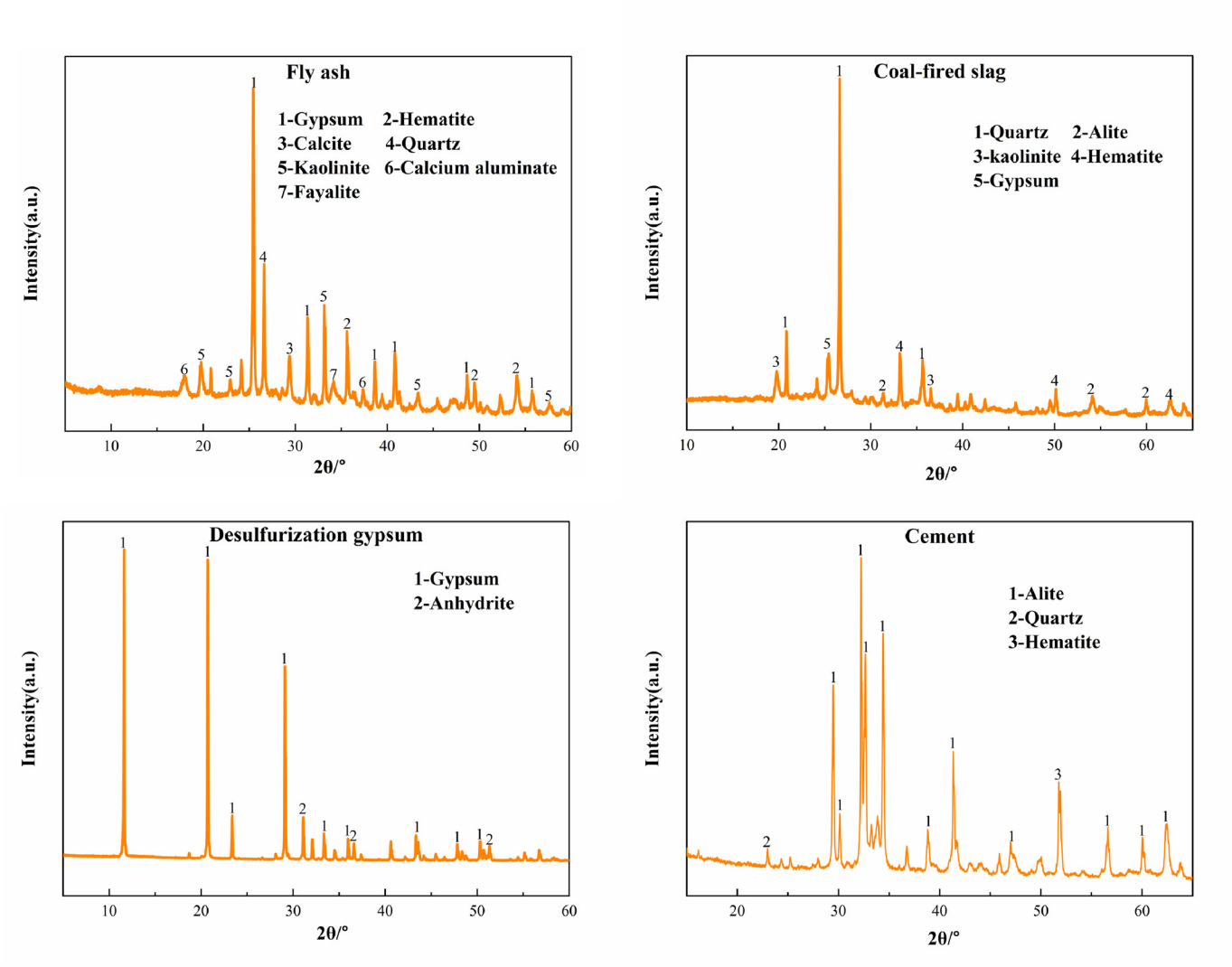

Figure 1. XRD patterns of raw materials.

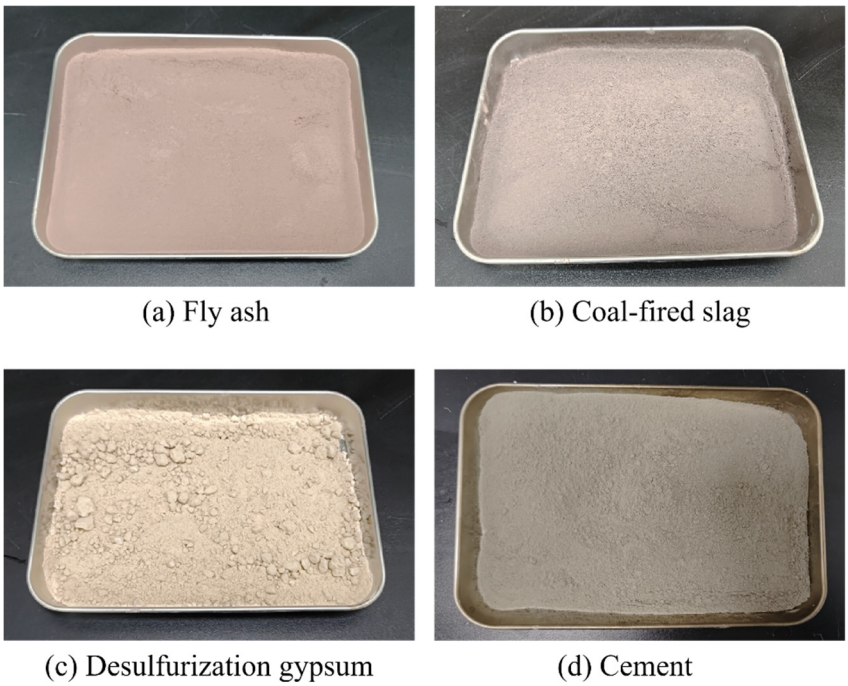

Figure 2. Macroscopic morphology of raw materials.

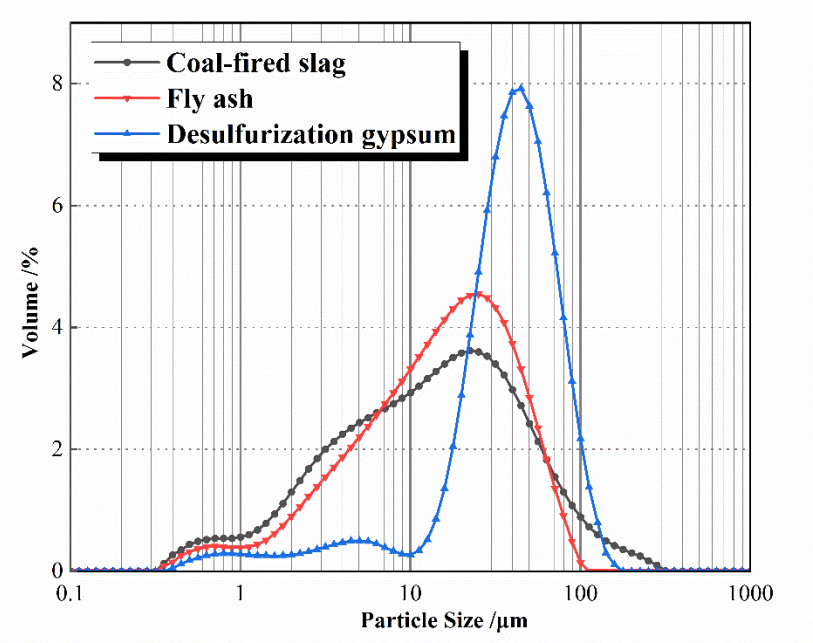

Figure 3. Analysis of particle size of solid waste from thermal power plants.

In accordance with GB/T 1346-2024 Standard Test Methods for Water Requirement for Standard Consistency, Setting Time and Stability of Cement, GB/T 17671-2021 Standard Test Methods for Strength of Cement Mortar (ISO Method), and GB/T 1345-2005 Test Method for Fineness of Cement—Sieve Analysis Method to evaluate the performance of the test cement, with results presented in Table 2.

Table 2. Analysis of Cement Properties.

Residue (0.08 mm) /%	Water /%	Stability	Initial Setting Time /min	Final Setting Time /min	Flexural Strength /MPa		Compressive Strength /MPa	
					7d	28d	7d	28d
1.6	26	Qualified	120	165	8.1	12.9	27.4	44

The 7d and 28d reactivities of FA used in this test were evaluated in accordance with GB/T 1596-2017 Fly Ash for Cement and Concrete. The results are presented in Table 3. The 7d and 28d reactivity values were 48.8% and 58.4%, respectively, meeting the Grade III FA standard and classifying it as low-reactivity FA. The low reactivity of FA is due to its low CaO content and the encapsulation of active silica-alumina components by glass phase, which makes it difficult to participate in the early hydration reaction and can only be slowly activated in the alkaline environment constructed by cement and CS in the later stage.

Table 3. Analysis of FA activity.

Group	Cement /g	Fly Ash /g	Standard Sand /g	Water /mL	Compressive Strength /MPa		Activity /%	
					7d	28d	7d	28d
Blank	450	0	1350	225	29.3	43.5	-	-
Experimental	315	135	1350	225	14.3	25.4	48.8	58.4

2.2. Experimental Design

This experiment employs CS (factor A), DG (factor B), and Cement (factor C) as independent variables, with three levels assigned according to their blending ratios. The FA blending ratio is set as the matrix component (with its content adjusted to 100% minus the sum of CS, DG, and cement), while the 7d and

28d compressive strengths of the FA-based composite cementitious material constitute response values Y_1 and Y_2, respectively. Preliminary experiments determined optimal addition ranges for CS, DG, and cement as 15–25%, 5–15%, and 10–20%, respectively. The independent variables and their levels are shown in Table 4. The setting of the factor level range is based on the chemical characteristics of each raw material: the low addition of DG cannot provide enough SO_4^{2-} for AFt formation, while the excessive addition will cause systemic supersaturation; the low addition of CS lacks sufficient silicate components for late gel formation, while the excessive addition will reduce the early alkaline environment of the system; the low addition of cement fails to form an effective alkaline activation environment, while excessive addition will lead to excessive early hydration heat and increased porosity.

Table 4. Response surface factor—level.

Level	A	B	C
−1	15	5	10
0	20	10	15
+1	25	15	20

2.3. Sample Preparation

CS, DG, cement, and FA were added to a cement ball mill in the proportions specified in Table 5 and ground thoroughly for 40 min. Subsequently, 450 g of the blended cementitious material was prepared for each sample group, the ground cementitious materials were mixed with standard sand and water in the proportions specified by GB/T 17671-2021 (ISO Method) for the Test Method of Cement Mortar Strength using a cement mortar mixer until thoroughly and uniformly blended. The mortar was poured into triple cement mortar molds measuring 40 mm × 40 mm × 160 mm. Repeatedly tapped the mold several times to expel air bubbles from the paste. The molds were placed in a constant temperature and humidity curing chamber (20 °C, 90% relative humidity) for 24 h prior to demolding. Subsequently, the test specimens were placed in the curing chamber for continued curing at 20 °C and 90% relative humidity for 7d and 28d.

Table 5. Ratio of fly ash-based cementitious materials.

Sample	A	B	C	Coal-Fired Slag/%	Desulfurization Gypsum/%	Cement/%	Fly Ash/%
1	−1	−1	0	15	5	15	65
2	+1	−1	0	25	5	15	55
3	−1	+1	0	15	15	15	55
4	+1	+1	0	25	15	15	45
5	−1	0	−1	15	10	10	65
6	+1	0	−1	25	10	10	55
7	−1	0	+1	15	10	20	55
8	+1	0	+1	25	10	20	45
9	0	−1	−1	20	5	10	65
10	0	+1	−1	20	15	10	55
11	0	−1	+1	20	5	20	55
12	0	+1	+1	20	15	20	45
13	0	0	0	20	10	15	55
14	0	0	0	20	10	15	55
15	0	0	0	20	10	15	55
16	0	0	0	20	10	15	55
17	0	0	0	20	10	15	55

3. Results and Discussion

Using the Box-Behnken response surface methodology, 17 orthogonal experimental designs were formulated based on three independent variables. Experimental data and the compressive strengths of cement mortar at 7d and 28d are presented in Table 6. Groups 13 to 17 comprised replicate experiments at zero points, undertaken to minimize data error.

Table 6. Testing of the mechanical properties of cement mortar specimens.

Sample	A	B	C	Compressive Strength/MPa	
				7d	28d
1	−1	−1	0	9.8	15.5
2	+1	−1	0	10.5	16.1
3	−1	+1	0	12.0	15.9
4	+1	+1	0	12.2	17.4
5	−1	0	−1	10.0	15.7
6	+1	0	−1	10.7	16.6
7	−1	0	+1	11.8	16.3
8	+1	0	+1	12.2	17.6
9	0	−1	−1	9.5	14.6
10	0	+1	−1	10.9	16.9
11	0	−1	+1	11.2	17.2
12	0	+1	+1	12.8	16.2
13	0	0	0	13.5	18.7
14	0	0	0	13.6	18.6
15	0	0	0	13.2	18.8
16	0	0	0	13.4	18.8
17	0	0	0	13.7	18.7

3.1. Response Surface Modelling and Significance Analysis

Using Design-Expert 13 software to fit quadratic regression curves yielded the second-order response surface regression equations for independent variables A, B, C, and their interaction terms with Y_1 and Y_2. The fitting equations for Y_1 and Y_2 are as follows:

$$Y_1 = -27.0175 + 1.969A + 1.2145B + 1.6105C - 0.005AB - 0.003AC + 0.002BC - 0.0456A^2 - 0.0486B^2 - 0.046C^2 \quad (1)$$

$$Y_2 = -20.2075 + 1.6935A + 1.518B + 1.6395C + 0.009AB + 0.004AC - 0.033BC - 0.0434A^2 - 0.0564B^2 - 0.0434C^2 \quad (2)$$

The correlation coefficients R^2 of Y_1 and Y_2 are 0.9918 and 0.9979, respectively, with the adjusted R^2(R^2_{adj}) values of 0.9812 and 0.9951 (Table 7). This indicates excellent model correlation, with predicted values closely matching actual values. Although the model shows an extremely high regression fit, it must be acknowledged that such a high R^2 value may pose a certain risk of overfitting. This is a common issue in small-sample quadratic polynomial regression modeling (17 groups in this study). The high fitting degree of the model provides a solid statistical foundation for subsequent correlation of the factor effect laws with the hydration mechanism and microstructure evolution.

Table 7. Significance analysis of predictive models.

Age	*C.V.*%	R^2	R^2_{Adj}	F-Value	*p*-Value	Significance
7d	1.65	0.9918	0.9812	93.58	<0.0001	Highly significant
28d	0.54	0.9979	0.9951	364.06	<0.0001	Highly significant

The *p*-values for Y_1 and Y_2 are both less than 0.0001, indicating that the model is highly significant. The coefficients of variation for Y_1 and Y_2 are both less than 5%, demonstrating that the experimental results are highly reliable.

Plots were generated to compare the predicted compressive strengths at 7d and 28d with their actual values, thereby further validating the data accuracy and model precision, as shown in Figure 4. It is evident that the predicted values for the 7d and 28d compressive strengths of the composite cementitious material closely approximate the actual values, with the 28d predicted values exhibiting a higher degree of proximity. Consequently, employing this response model to predict the 7d and 28d compressive strengths of FA-based composite cementitious materials is highly feasible.

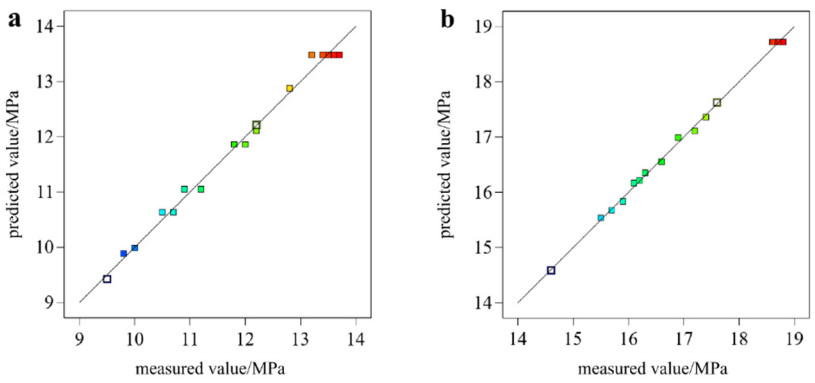

Figure 4. Predicted and measured compressive strength values: (**a**) 7d; (**b**) 28d.

3.2. Prediction Variance Analysis and Significance Testing

To investigate the extent to which each independent variable and its interactions influence the compressive strength of cementitious materials, variance analysis was conducted on the established regression models. The results are presented in Table 8. The variance analysis results of the model are the key basis for analyzing the differential effects of each factor on strength at different ages, and the corresponding hydration reaction and microstructural evolution mechanism can explain each statistical result.

Table 8. Analysis of variance for the response value prediction model.

Response Value	Source	Squares	Mean Square	F-Value	*p*-Value	Significance
Y_1	*A*	0.5	0.5	13.18	0.0084	Significant
	B	5.95	5.95	156.91	<0.0001	Highly significant
	C	5.95	5.95	156.91	<0.0001	Highly significant
	AB	0.0625	0.0625	1.65	0.2401	
	AC	0.0225	0.0225	0.5932	0.4664	
	BC	0.01	0.01	0.2637	0.6234	
	A^2	5.47	5.47	144.27	<0.0001	Highly significant
	B^2	6.22	6.22	163.88	<0.0001	Highly significant
	C^2	5.71	5.71	150.67	<0.0001	Highly significant
Y_2	*A*	2.31	2.31	267.42	<0.0001	Highly significant
	B	1.13	1.13	130.17	<0.0001	Highly significant
	C	1.53	1.53	177.17	<0.0001	Highly significant
	AB	0.2025	0.2025	23.43	0.0019	Significant
	AC	0.04	0.04	4.63	0.0685	
	BC	2.72	2.72	315	<0.0001	Highly significant
	A^2	4.96	4.96	573.51	<0.0001	Highly significant
	B^2	8.37	8.37	968.54	<0.0001	Highly significant
	C^2	4.96	4.96	573.51	<0.0001	Highly significant

3.2.1. 7d Compressive Strength Response Model (Y_1)

As shown in Table 8, the *p*-values for independent variables *A*, *B*, and *C* are 0.0084, <0.0001, and <0.0001, respectively, all of which are less than 0.05. This indicates that all three factors exert a significant influence on the 7d compressive strength. Among these, the effects of factors *B* and *C* were more pronounced ($p < 0.0001$), indicating that *B* and *C* play a dominant role in the development of early-stage strength. From the perspective of hydration mechanism, this statistical result is due to the fact that cement and DG are the core driving factors of the early hydration reaction: cement dissolves rapidly in water to release a large amount of Ca^{2+} and OH^-, a large amount of CH is produced in the reaction, which rapidly constructs a strong alkaline environment for the system, and at the same time forms initial C-S-H gel to provide early-stage strength. DG decomposes to release SO_4^{2-}, which reacts with Ca^{2+} and AlO_2^- in the alkaline environment to form AFt crystals, AFt crystals have a needle-like structure, which can fill the internal pores of the material in the early stage and significantly improve the early compressive strength of the system. The *p*-values for the interaction terms *AB*, *AC*, and *BC* are all greater than 0.05, indicating that the interaction effects between the factors exert a relatively minor influence on the 7d strength. This is because the early hydration reaction of the system is dominated by the rapid dissolution and reaction of cement and DG, and the CS with low early activity has not yet participated in the reaction in large amounts, so the interaction between the factors is not obvious in the early stage. The *p*-values for A^2, B^2, and C^2 are all less than 0.001, reaching a highly significant level. This indicates that the 7d compressive strength exhibits a pronounced non-linear relationship with variations in each factor, and that curvature effects are present in the response surface. The non-linear effect is due to the fact that excessive addition of any factor will destroy the balance of the early hydration reaction: excessive cement leads to excessive hydration heat and increased porosity; excessive DG causes SO_4^{2-} supersaturation and inhibits the formation of AFt crystals; excessive CS dilutes the content of cement and DG, reducing the amount of early hydration products.

3.2.2. 28d Compressive Strength Response Model (Y_2)

As shown in Table 8, the *p*-values for factors *A*, *B*, and *C* are all less than 0.0001, indicating that each factor significantly influences the 28d compressive strength. Notably, the F-value of factor A (CS) is 267.42, which is the highest among the three factors, indicating that CS has become the dominant factor regulating the late strength of the system, which is consistent with the microstructural characteristics results of hydration products. The interaction terms *AB* ($p = 0.0019$) and *BC* ($p < 0.0001$) exerted significant effects, indicating pronounced synergistic or inhibitory interactions between certain factors during the later stages of the hydration process. The significant interaction between factors in the later stage is due to the fact that the hydration reaction of the system has entered the synergistic activation stage, and CS, DG, and cement participate in the reaction together and restrict each other. The *p*-values for A^2, B^2 and C^2 were all less than 0.0001, indicating that each independent variable exerted a significant influence on the later-stage strength. It is thus evident that the development of 28d compressive strength was markedly affected not only by the individual main effects but also by the combined influence of interactions between factors. The reason why CS dominates the 28d strength is closely related to its chemical composition and the slow pozzolanic reaction characteristics: first, CS is rich in CaO and silicate components, and under the alkaline environment constructed by cement hydration in the early stage, its surface glass phase is gradually eroded by OH^-, and the internal active SiO_2 and Al_2O_3 are continuously released; second, the active silica-alumina components released from CS react with CH generated by cement hydration to produce a large amount of C-S-H and C-(A)-S-H gel in the later stage, This kind of secondary hydration gel has a denser structure and better cementing performance than the early C-S-H gel generated by cement hydration; third, the continuous generation of C-S-H gel in the later stage can fill the internal pores of the material, reduce the porosity, and make the microstructure of the cementitious material more compact, thus significantly improving the late

compressive strength. In addition, CS can also slowly activate the low-reactivity FA in the system at a later stage, promoting the FA to participate in the hydration reaction and generate more gel products, forming a synergistic activation effect with FA.

3.2.3. Model Comparison and Analysis

In summary, the regression equations of both response models exhibit high significance and reliability, indicating that the established quadratic polynomial model effectively reflects the quantitative relationships between various factors and compressive strength. Comparatively, the 7d strength is primarily governed by single factors and quadratic terms, exhibiting a distinctly unimodal response trend. This is because the early hydration reaction is a rapid dissolution and direct reaction process, and the strength development is mainly determined by the amount of early hydration products (AFt, initial C-S-H gel) generated by cement and DG. Beyond the main effect, certain interaction terms for the 28d strength were also significant, indicating that the development of long-term strength is influenced by the complex interplay of multiple factors. The late strength development is a synergistic activation process of multiple materials: CS is the core source of late gel formation, DG provides continuous SO_4^{2-} to maintain the stability of AFt crystals, and cement provides a continuous alkaline environment for the pozzolanic reaction of CS and FA, these three factors interact and constrain each other, and jointly regulate the late-stage strength. The high significance of the quadratic terms suggests that each factor within the system exhibits an optimal range for influencing strength, demonstrating the feasibility of employing response surface methodology to determine optimal formulation parameters. The optimal range of each factor is the result of the balance of hydration reactions at different stages: the optimal content of cement can construct a suitable alkaline environment for early and late reactions; the optimal content of DG can ensure the rapid formation of AFt in the early stage and avoid supersaturation in the late stage; the optimal content of CS can ensure the sufficient generation of late gel without diluting the early hydration products.

3.3. The Interactive Effect of CS and DG Content on Y_1 and Y_2

Figure 5 presents the response surfaces and contour plots illustrating the effects of independent variables CS (A) and DG (B) on the compressive strength of FA-based cementitious materials at 7d and 28d. As illustrated in the figure, the combined effect of both factors on compressive strength exhibits a typical quadratic surface morphology. The response surface is generally smooth with distinct peak regions, indicating that both factors possess optimal values. A significant non-linear relationship exists between each factor and strength within the system.

As observed in Figure 5a,b, the 7d compressive strength initially increases and then decreases with rising CS and DG contents, exhibiting a unimodal variation trend. The response surface displays a pronounced convex profile, indicating a synergistic enhancement effect between the two factors within a moderate range. When both CS and DG content are at moderate levels, the system's early-stage strength reaches its maximum value; beyond this range, strength actually decreases. This is primarily attributable to the dual effect of the active CS products on the equilibrium between SO_4^{2-} and Ca^{2+} within the DG-regulated system. An appropriate amount of DG promotes the pozzolanic reaction, generating more C-S-H gel; however, excessive DG leads to supersaturation within the system, thereby inhibiting the effective formation of hydration products [27]. A small amount of CS can provide a small amount of Ca^{2+} to cooperate with DG to form AFt, but excessive CS will reduce the content of DG and cement in the system, resulting in insufficient early hydration products. Within the 7d system, the response curve for DG shows a steeper gradient. This indicates that DG exerts a greater influence on the 7d compressive strength than CS does. This occurs because DG reacts initially with water to form CH and C-S-H gel or crystalline

substances. These reactions hydrate rapidly, contributing significantly to early-stage strength development. Consequently, the proportion of DG added to the system exerts a more pronounced effect.

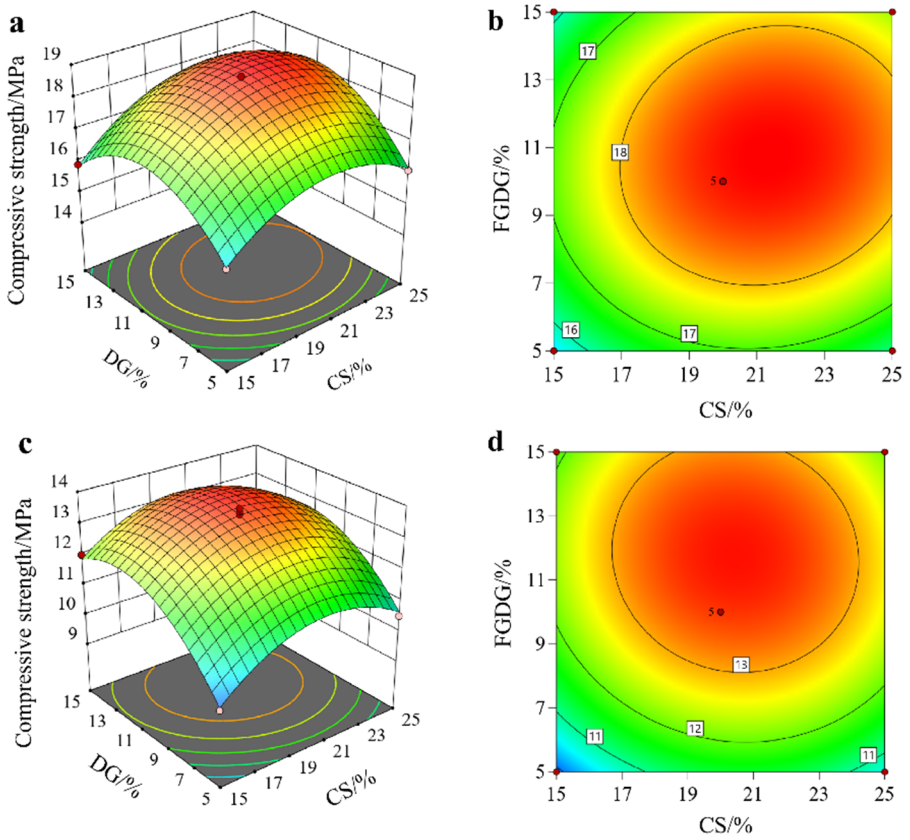

Figure 5. Influence of the interaction between coal-fired slag and desulfurization gypsum on compressive strength of composites: (**a**) 7d response surface plot; (**b**) 7d contour lines; (**c**) 28d response surface plot; (**d**) 28d contour lines.

As can be seen from Figure 5c,d, the response surface for the 28d compressive strength also exhibits a pronounced quadratic effect. The surface is more gently sloping with a relatively broad peak region, indicating that the system's sensitivity to mix proportions decreases during prolonged hydration. This is because the system has formed a dense microstructure in the late stage, and small changes in factor content have a relatively small impact on the strength. As the CS content increases, compressive strength initially rises before declining. Moreover, the response curve on the CS side exhibits a steeper gradient and more densely spaced contour lines. This indicates that CS exerts a more pronounced influence on later-stage strength development. This statistical characteristic is essentially due to the fact that CS is the core factor of late gel formation: the increase of CS content within the optimal range can provide more active silica-alumina components for the late pozzolanic reaction, generate more C-S-H gel, and significantly improve the late strength; excessive CS will lead to the reduction of cement content, the weakening of the alkaline environment of the system, and the inhibition of the pozzolanic reaction of CS itself and FA. An appropriate amount of DG maintains the continuous progression of the aluminum sulfate reaction within the system. The alkaline substances provided, such as calcium hydroxide, promote the hydration reactions of CS and FA, thereby facilitating the formation of C-S-H and C-(A)-S-H gels [28]. When the dosage of DG exceeds the optimum level, the initial hydration reaction proceeds too rapidly, resulting in excessive water absorption. This leads to a significant shortage of free water required for subsequent hydration, causing a decline in strength.

3.4. The Interactive Effect of CS and Cement Content on Y_1 and Y_2

Figure 6 presents the response surfaces and contour plots illustrating the effects of CS content (A) and cement dosage (C) on the compressive strength of FA-based cementitious materials at 7d and 28d. As evident from the figure, both response surfaces exhibit a typical quadratic parabolic shape, with contour lines distributed in a relatively concentrated, near-elliptical pattern. This indicates that both factors in the system exert a significant quadratic effect on compressive strength, which follows a distinct pattern of initial increase followed by a decrease with variations in cement content.

In Figure 6a, the response surface on the cement side exhibits a steeper gradient, with contour lines densely distributed from the periphery towards the center. This indicates that cement content has a more significant effect on the 7d strength of the system. This occurs because the substantial calcium oxide present in the cement reacts initially with water to form calcium hydroxide (CH), progressively enhancing the alkalinity of the system. Subsequently, CH reacts with SiO_2 and Al_2O_3 to form C-S-H and C-(A)-S-H. The consumption of CH further promotes the cement hydration reaction. As the proportion of CS and cement increases, strength gradually reaches a peak before declining. This phenomenon indicates that during the early age period, an appropriate amount of cement provides sufficient OH^- ions to promote CS activation reactions, thereby forming a greater quantity of C-S-H gel and enhancing structural density. However, when the cement content becomes excessively high, the system experiences intensified hydration exothermic reactions and increased porosity, which conversely diminishes the strength-enhancing effect [29]. Excessive cement also leads to the rapid consumption of free water in the system, resulting in incomplete hydration of cement particles and the formation of internal microcracks, which reduce the early-stage strength.

As can be seen from Figure 6c,d, the response surface for the 28d compressive strength is more gradual than that for the 7d strength, with contour lines distributed more sparsely. This indicates that the influence of cement and CS content variations on later-stage strength diminishes relatively. With increasing proportions of both materials, the mechanical strength of the mortar also exhibits a trend of initial increase followed by decline. However, the peak region is closer to the CS side, indicating that later-stage strength is more susceptible to variations in CS content. The CH produced by cement hydration reacts with pozzolanic substances in the CS, reducing the CH content in the hydration liquid phase. This in turn accelerates cement hydration, creating a self-reinforcing cycle that continuously promotes pozzolanic reactions and generates more late-stage gel phases. Consequently, the response curve on the CS side exhibits a steeper gradient [30]. This self-reinforcing cycle is the key reason for the synergistic effect of cement and CS on the late strength: cement provides CH for the pozzolanic reaction of CS, and the consumption of CH promotes the further hydration of cement, forming a positive cycle of hydration reaction. Concurrently, the CH provided by the cement serves as a reaction initiator to sustain the system's activity. Should the cement content be excessive, the resulting elevated alkalinity and accelerated reaction rate may induce increased microcracking within the structure, leading to a slight reduction in later-stage strength. Excessive CS will also dilute the cement content, leading to an insufficient alkaline environment in the system, inhibiting the pozzolanic reaction of CS and FA, and reducing the amount of late gel products.

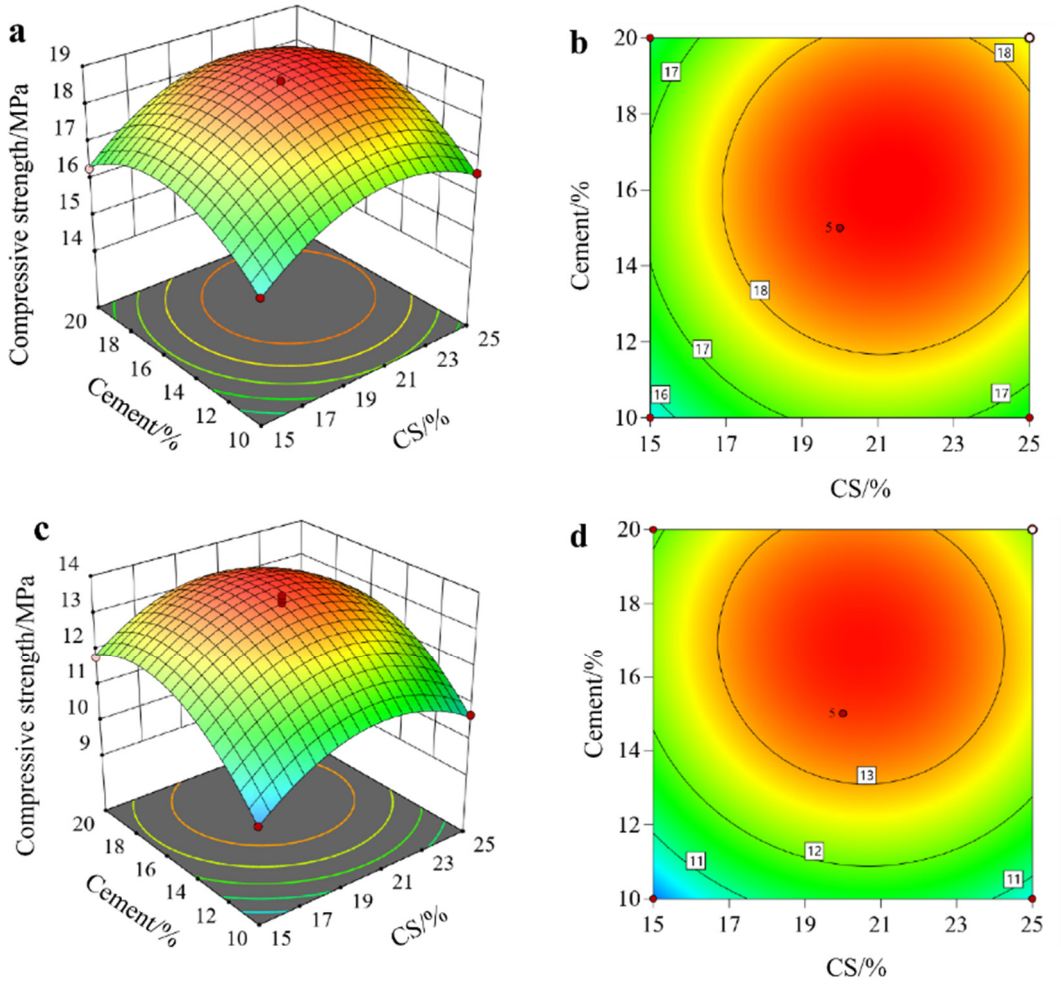

Figure 6. Influence of the interaction between coal-fired slag and cement on compressive strength of composites: (**a**) 7d response surface plot; (**b**) 7d contour lines; (**c**) 28d response surface plot; (**d**) 28d contour lines.

3.5. The Interactive Effect of DG and Cement Content on Y_1 and Y_2

Figure 7 presents the response surface and contour plots illustrating the effects of DG (B) and cement dosage (C) on the 7d and 28d compressive strength of FA-based cementitious materials. The figure demonstrates that both DG and cement content exert a pronounced influence on the system's strength. The response surface exhibits a sharp peak profile, with denser contour lines converging towards an elliptical center. Strength follows an initial increase followed by a subsequent decrease, indicating that variations in these parameters significantly impact the system's strength.

In Figure 7a,b, the density of contour values for cement and DG content is approximately equal. This indicates that both materials contribute similarly to the early-stage hydration reaction. This is because both DG and cement contain substantial amounts of calcium oxide, which generates significant quantities of CH and C-S-H gel during the initial hydration phase. Both substances contribute significantly to early-stage strength development. Cement provides Ca^{2+} and OH^- for the early hydration reaction, the two factors cooperate to form AFt crystals and initial C-S-H gel, which are the two main sources of early-stage strength, so their influence on early-stage strength is basically the same. When the dosage of both components is too low, the system exhibits reduced strength due to insufficient alkali activators. Conversely, when their dosage is excessive, the high calcium oxide content causes overly vigorous hydration reactions, leading to incomplete hydration and cracking, resulting in strength decline. Cement provides Ca^{2+}, and OH^- for the early hydration reaction, and DG provides SO_4^{2-}. The two factors cooperate to form AFt crystals and initial C-S-H gel, which are the two main sources of early-stage strength, so their influence on early-stage strength

is basically the same. Figure 7c,d demonstrate that cement dosage exerts a more pronounced effect on 28d compressive strength. This occurs because excessive DG content promotes the formation of calcium sulfate dihydrate during hydration. This compound possesses a loose structure and weak bonding properties, leading to dissolution under water immersion. Consequently, strength diminishes, compromising the material's capacity to sustain long-term high-strength stability [31].

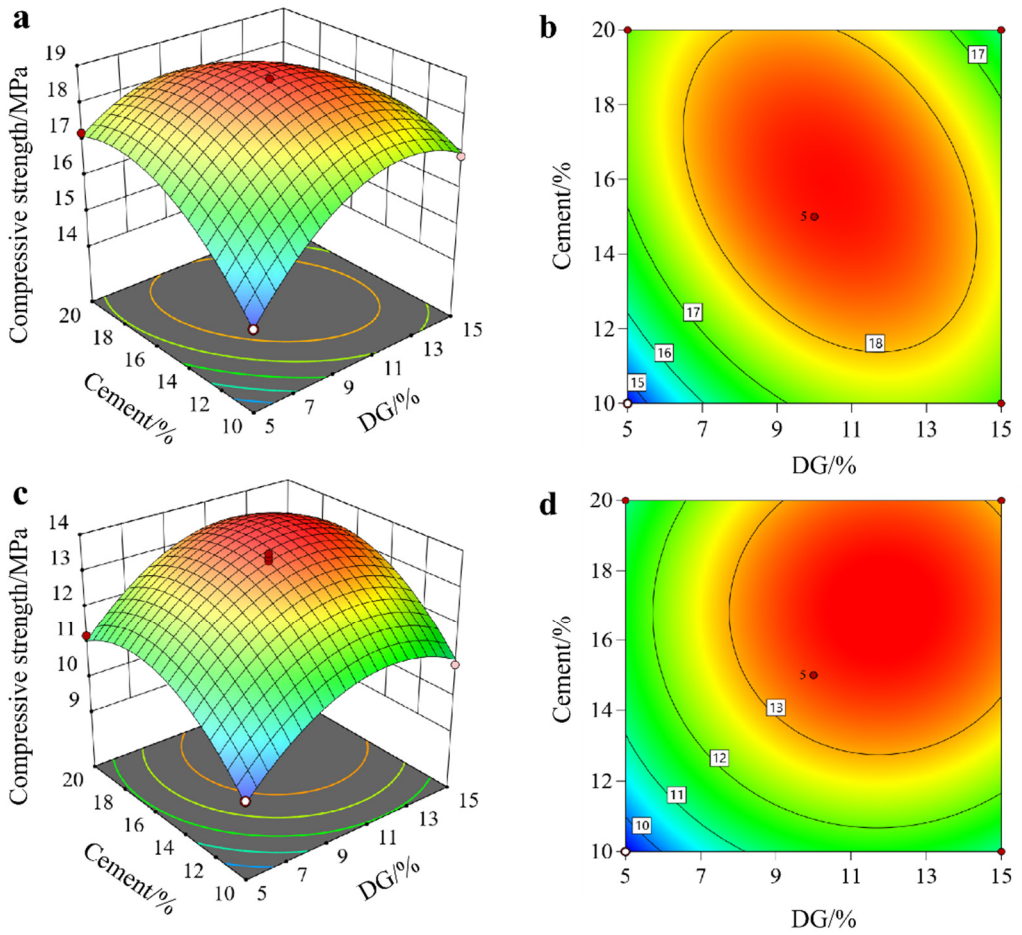

Figure 7. Influence of the interaction between desulfurization gypsum and cement on compressive strength of composites: (**a**) 7d response surface plot; (**b**) 7d contour lines; (**c**) 28d response surface plot; (**d**) 28d contour lines.

3.6. Experimental Verification

To validate the practical application effectiveness of the response model, taking the 7d and 28d compressive strengths as verification indices, the optimal mix ratio obtained from the response surface model was used as the optimized group. The optimal mix ratio was determined as 21.38% CS, 10.96% DG, 16.15% cement, with FA accounting for the remainder. The compressive strengths of mortar at 7d and 28d were measured for the optimized group. Experimental results are presented in Table 9. The data indicate relative deviations of 0.80% and 1.27% for the 7d and 28d optimized groups, respectively, demonstrating the model's high predictive accuracy. The optimal mix ratio is the optimal balance point of the hydration reaction at different stages: 16.15% cement can construct a suitable alkaline environment for early and late reactions without excessive hydration heat; 10.96% DG can provide sufficient SO_4^{2-} for early AFt formation and avoid late supersaturation; 21.38% CS can ensure the sufficient generation of late C-(A)-S-H gel and form a synergistic activation effect with FA, which is the statistical embodiment of the optimal hydration reaction balance from the perspective of mix proportion.

Table 9. Predicted and actual compressive strength for the optimal model at 7d and 28d.

Coal-Fired Slag /%	Desulfurization Gypsum /%	Cement /%	Fly Ash /%	7d Compressive Strength/MPa		28d Compressive Strength/MPa	
				Predicted	Actual	Predicted	Actual
21.38	10.96	16.15	51.51	13.71	13.60	18.83	19.07

3.7. Analysis of Hydration Mechanism

Figure 8 presents the XRD test results for the 7d and 28d hydration products of the optimized composite cementitious material. The test results reveal that the mineral composition of the hydration paste comprises inert minerals from the solid waste of thermal power plants coexisting with newly formed hydration products. Sharp diffraction peaks corresponding to inert mineral phases (quartz, hematite, and calcic pyroxene) were detected in both the 7d and 28d specimens. These phases originate from unreacted aggregates in FA and CS, functioning as the physical skeleton within the mortar. Comparing the XRD patterns of the two age stages reveals characteristic peaks of AFt crystals appearing at 28d. Upon magnification, a marked contrast in peak intensity is observed relative to the 7d stage. This arises from the earlier hydration reactions where DG, cement, and water react to generate substantial amounts of OH^- and Ca^{2+}. These ions react rapidly with SiO_2 and Al_2O_3 to form C_3S and C_3A. As hydration progresses, Ca^{2+} in the system is adsorbed by pozzolanic materials, while C_3S and C_3A gradually dissolve, releasing Al^{3+} and Ca^{2+}. These ions continuously accumulate with SO_4^{2-} to form Aft [32]. Moreover, distinct CH peak shapes are observable at 28d, indicating that as the hydration reaction progresses, well-formed CH crystals gradually develop.

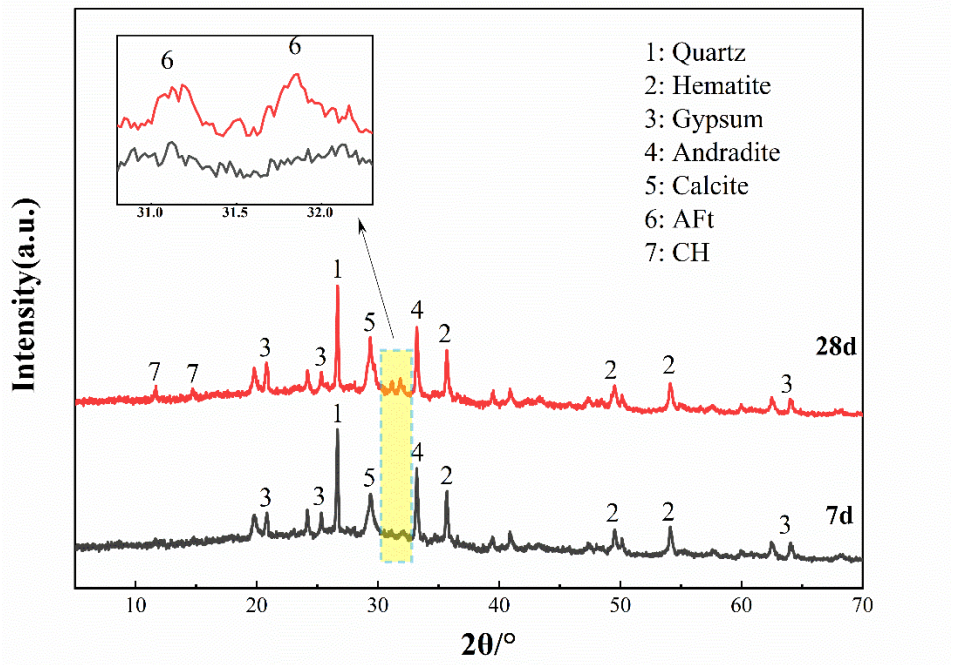

Figure 8. XRD diagram of optimized group composite cement paste.

Figure 9 presents SEM images of the hydration products of the optimized composite material at 7d and 28d. Figure 9a,b show SEM images of the 7d hydration products, while Figure 9c,d depict those of the 28d hydration products. During the initial curing period (7d), the hydration reactions within the cementitious system proceed at a rapid pace, resulting in a microstructure exhibiting significant inhomogeneity and porosity. Figure 9a reveals abundant early-formed flocculent or gel-like C-S-H. Figure 9b distinctly shows unreacted FA particles covered by substantial amorphous C-S-H gel. This structure is relatively loose,

without a continuous and dense skeletal framework; obvious pores and interfacial cracks exist between particle aggregates. This relatively loose microstructural characteristic explains the comparatively low early-stage mechanical strength of the filler [33]. As the curing age was extended to 28d, the hydration degree of the system was significantly enhanced, accompanied by pronounced changes in microstructure. Figure 9c clearly reveals well-developed hexagonal plate-like CH crystals and needle-like AFt crystals, consistent with the XRD analysis results presented in Figure 8. The emergence of these well-developed crystalline phases indicates that the hydration reaction has entered a stable phase. Compared to 7d, Figure 9d exhibits a more compact matrix structure, with abundant C-S-H gel tightly cementing crystals such as AFt and CH. This fills early-stage pores, forming a dense spatial network structure. Needle-like AFt crystals interweave within the C-S-H gel network, functioning as a microfiber-like framework [34]. Together with CH crystals, they constitute a robust spatial skeleton, explaining the enhanced macroscopic mechanical strength. The evolution of the aforementioned microstructure demonstrates that the hydration reaction within the system has proceeded to a considerable degree. The material proportions are scientifically sound and well-balanced, fully activating the pozzolanic substances within the FA and CS materials.

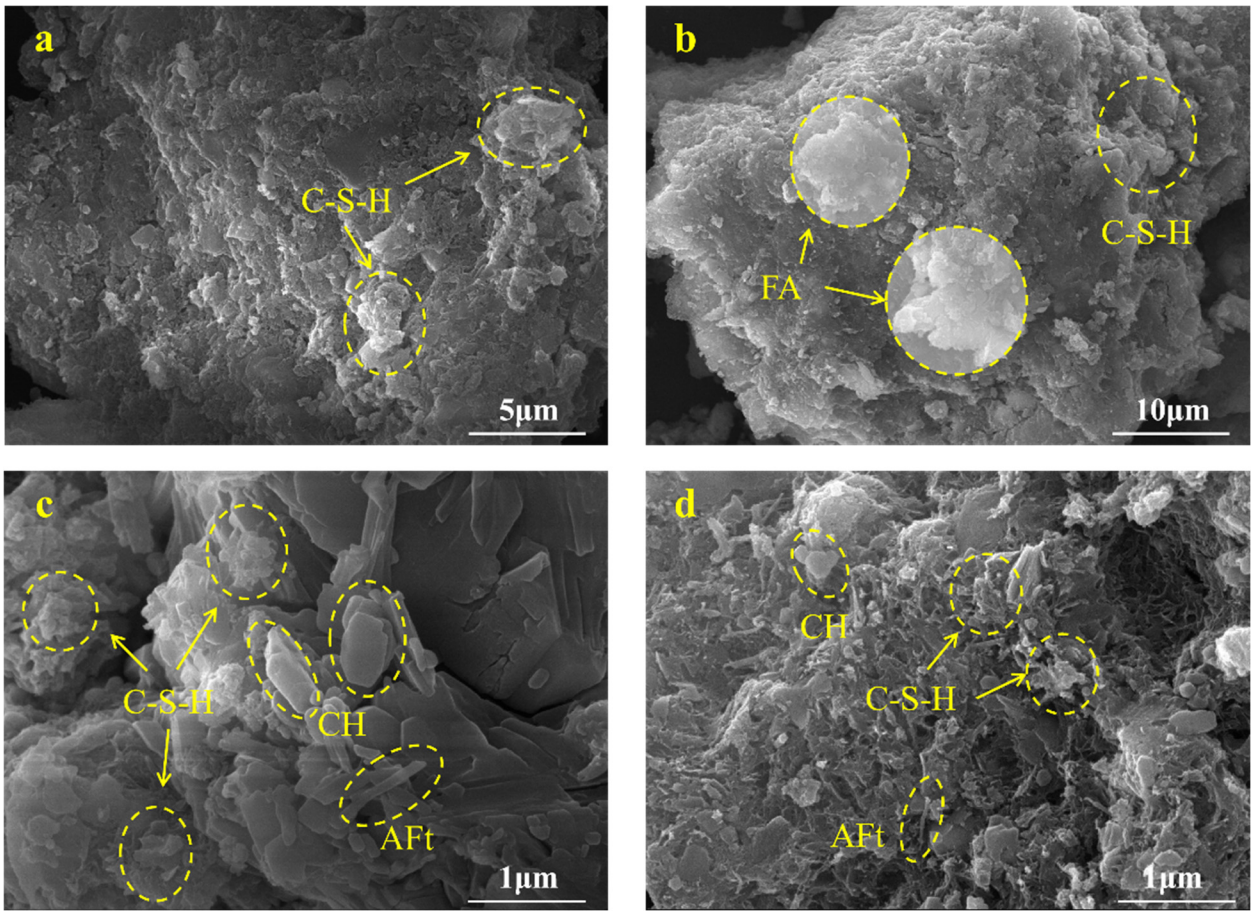

Figure 9. SEM Images of optimized cement paste: (**a**) 7d; (**b**) 7d; (**c**) 28d; (**d**) 28d.

4. Conclusions

In this study, the Box-Behnken response surface methodology was employed to establish a fly ash-based composite cementitious material system, with coal-fired slag (CS), desulfurization gypsum (DG), and cement as influencing factors and the 7d and 28d compressive strengths of mortar as response values. The effects of each factor on the response values and the hydration mechanism of the optimally proportioned material were investigated, with the main conclusions drawn as follows:

CS, DG, and cement in the FA-based composite cementitious system exert significant quadratic effects on compressive strength with obvious interactive characteristics; DG and cement are the dominant factors governing the 7d early-stage strength, while CS exerts a more significant effect on the 28d late-stage strength, which clarifies the differential regulation law of each component on the strength development of the system.

BBD demonstrates unique advantages: only 17 orthogonal experiments (including 5 replicate zero points) are required to comprehensively analyze the main effects, quadratic effects, and interactions of three factors, balancing experimental efficiency with optimization accuracy. The extremely low model coefficient of variation (C.V.) (1.65% at 7 days and 0.54% at 28 days) indicates high reproducibility of experimental results and robustness of the optimized formulation. This study demonstrates that the response surface method effectively avoids the blindness inherent in traditional mix design approaches, enabling precise control over material properties.

XRD and SEM characterization results show that the optimally proportioned system forms abundant C-(A)-S-H gels, hexagonal plate-like CH, and needle-like AFt at 28d. The hydration products form a dense spatial network structure, which fully activates the pozzolanic activity of low-reactivity FA and CS, and is the fundamental reason for the improvement of the macroscopic mechanical strength of the material.

5. Limitations and Future Directions

This study evaluated only the 7d and 28d compressive strength and basic hydration characteristics of the composite cementitious material. No relevant tests were conducted on long-term durability properties (e.g., dry shrinkage, water permeability, and carbonation resistance), which are key indicators for the practical engineering application of the material.

Furthermore, although the established Box-Behnken response surface model demonstrates high predictive accuracy for the experimental data in this study, it has currently been validated only through replicate zero-point experiments and optimal proportion verification experiments within the research dataset. It lacks validation using independent external datasets—a crucial step for ensuring the generalization capability of predictive models, particularly critical in related machine learning and regression modeling research.

Subsequent research will systematically test the long-term durability of the optimal proportion system and explore the evolution patterns of its microstructure and mechanical properties under different service environments. Concurrently, independent experimental datasets from diverse sources of thermal power solid waste and varying factor levels will be collected to validate and optimize the established response surface model. This will alleviate the potential impact of model overfitting on its generalization ability, further enhancing the model's applicability and predictive reliability across different engineering practice scenarios. This work will further refine the theoretical framework for the synergistic utilization of solid waste from thermal power plants, providing more comprehensive and reliable technical support for its engineering applications.

Acknowledgments

Special thanks to Wu Z.J. and Xie X.Q. for their generous support of this research. We also extend our gratitude to our colleagues in the laboratory for their assistance and support.

Author Contributions

H.X.: Writing-original draft, Supervision, Conceptualization, Data curation. L.Z.: Writing—original draft, Investigation, Data curation. Z.Z. (Ziyu Zou): Writing—review & editing, Data curation. Z.Z. (Zecheng Zeng): review & editing, investigation. M.Z.: Investigation, Funding acquisition. Z.W.: Funding

acquisition, Resources, Writing—review & editing, Project administration. X.X.: Writing—review & editing, Visualization.

Ethics Statement

Not applicable.

Informed Consent Statement

Not applicable.

Data Availability Statement

The statement is required for all original articles which informs readers about the accessibility of research data linked to a paper and outlines the terms under which the data can be obtained.

Funding

This work was supported by the Yuelu Mountain Industrial Innovation Center Project in Changsha, China (2024YCII0104) and the Central Government Guidance Fund for Local Science and Technology Special Projects in China (2024ZYC022).

Declaration of Competing Interest

The authors declare that they have no known competing financial interests or personal relationships that could have appeared to influence the work reported in this paper.

References

1. Bo L, Yang S, Liu Y, Zhang Z, Wang Y, Wang Y. Coal Mine Solid Waste Backfill Process in China: Current Status and Challenges. *Sustainability* **2023**, *15*, 13489. DOI:10.3390/su151813489
2. Falah M, MacKenzie KJD. Photocatalytic Nanocomposite Materials Based on Inorganic Polymers (Geopolymers): A Review. *Catalysts* **2020**, *10*, 1158. DOI:10.3390/catal10101158
3. Barbhuiya S, Das BB, Kapoor K, Das A, Katare V. Mechanical performance of bio-based materials in structural applications: A comprehensive review. *Structures* **2025**, *75*, 108726. DOI:10.1016/j.istruc.2025.108726
4. Li H, Zhang N, Yang J, Huang G, Lu M, Wang L. Chapter 17—Recycling of Textile and Fiber Wastes as Construction Materials. In *Wastes to Low-Carbon Construction Materials*; Wang L, Guo B, Ma B, Eds.; Woodhead Publishing: Cambridge, UK, 2025; pp. 521–560. Available online: https://www.sciencedirect.com/science/article/pii/B9780443273421000130 (accessed on 5 March 2026).
5. Li H, Zhang N, Yang J, Wang L, Köberle T, Mechtcherine V. Synergistic reinforcement of recycled carbon fibers and biochar in high-performance, low-carbon cement composites: A sustainable pathway for construction materials. *Cem. Concr. Compos.* **2025**, *162*, 106148. DOI:10.1016/j.cemconcomp.2025.106148
6. Han X, Mu Z, Wang Z. Optimization control and economic evaluation of energy storage combined thermal power participating in frequency regulation based on multivariable fuzzy double-layer optimization. *J. Energy Storage* **2022**, *56*, 105927. DOI:10.1016/j.est.2022.105927
7. Wang P, Hu B, Tai N, Zhao L, Vafai K. Peak shaving auxiliary service analysis for the photovoltaic and concentrating solar power hybrid system under the planning-dispatch optimization framework. *Energy Convers. Manag.* **2023**, *295*, 117609. DOI:10.1016/j.enconman.2023.117609
8. Xu Z, Li C, Xiao B, Chen G. Development of slag-based filling cementitious materials and their application in ultrafine tailing sand filling. *Constr. Build. Mater.* **2024**, *452*, 138966. DOI:10.1016/j.conbuildmat.2024.138966
9. Ruan S, Liu L, Zhu M, Shao C, Xie L, Hou D. Application of desulfurization gypsum as activator for modified magnesium slag-fly ash cemented paste backfill material. *Sci. Total Environ.* **2023**, *869*, 161631. DOI:10.1016/j.scitotenv.2023.161631
10. Zhang P, Wu F, Gao Q, Zhang T, Wang Y, Qi X. Use of coal-fired slag in filling bodies with early strength for mining applications. *J. Clean. Prod.* **2023**, *414*, 137465. DOI:10.1016/j.jclepro.2023.137465

11. Zhang X, Zhang X, Shuai P, Su L, Cai G. Mechanical properties and microscopic characteristics of fly ash–slag composite backfill. *Geomech. Geophys. Geo-Energy Geo-Resour.* **2023**, *9*, 132. DOI:10.1007/s40948-023-00664-7
12. Chu F, Li C, Wu C, Wang Y. Research on the hydration process of solid waste–based cementitious materials and application in roadbase. *Front Energy Res* **2024**, *11*, 1348557. DOI:10.3389/fenrg.2023.1348557
13. Zhou J, Chen S, Das AK. Application of sludge as a sustainable material in building materials: A comprehensive review. *J. Build. Eng.* **2025**, *111*, 113434. DOI:10.1016/j.jobe.2025.113434
14. Das AK. Natural sea-based materials SBM-ECCs: Experimental, analytical, and machine learning approaches to early-age behavior and modulating factors. *Appl. Soft Comput.* **2026**, *186*, 114101. DOI:10.1016/j.asoc.2025.114101
15. Sahani K, Timsina AP, Tuladhar B, Sahani SK, Kumar Das A. Low cost upcycling of non-segregated plastic waste as building materials in Nepal: Experimental investigation and microstructural analysis. *Constr. Build. Mater.* **2025**, *492*, 142955. DOI:10.1016/j.conbuildmat.2025.142955
16. Das AK, Qi Y. High performance natural seawater coral sand ECC (HP-NSCS-ECC) in coastal conditions: Experimental characterization, microstructure, and sustainability. *Constr. Build. Mater.* **2025**, *499*, 143860. DOI:10.1016/j.conbuildmat.2025.143860
17. Das AK, Qiu J, Leung CKY, Yu J. A novel strategy to assess healing induced recovery of mechanical properties(HIRMP) of strain hardening/engineering cementitious composites(SHCCs/ECCs) in autogenous healing. *Cem. Concr. Compos.* **2023**, *142*, 105177. DOI:10.1016/j.cemconcomp.2023.105177
18. Das AK, Leung CKY. A strategy for in situ determination of self-healing state for strain hardening cementitious composites. *Cem. Concr. Compos.* **2020**, *112*, 103641. DOI:10.1016/j.cemconcomp.2020.103641
19. Li G, Zhou C, Ahmad W, Usanova KI, Karelina M, Mohamed AM, et al. Fly Ash Application as Supplementary Cementitious Material: A Review. *Materials* **2022**, *15*, 2664. DOI:10.3390/ma15072664
20. Ge Y, Liu X, Shui Z, Gao X, Zheng W, Zhu Z, et al. Design and Preparation Technology of Green Multiple Solid Waste Cementitious Materials. *Materials* **2024**, *17*, 1998. DOI:10.3390/ma17091998
21. Amsalu Fode T, Jande YAC, Kivevele T. Modelling and optimization of multiple replacement of supplementary cementitious materials for cement composite by response surface method. *Clean. Eng. Technol.* **2024**, *19*, 100735. DOI:10.1016/j.clet.2024.100735
22. Li Z, Lu D, Gao X. Multi-objective optimization of gap-graded cement paste blended with supplementary cementitious materials using response surface methodology. *Constr. Build. Mater.* **2020**, *248*, 118552. DOI:10.1016/j.conbuildmat.2020.118552
23. Wang K, Fu J, Wang J. The ratio optimization and hydration mechanism of multi source solid waste cementitious materials. *Constr. Build. Mater.* **2024**, *411*, 134267. DOI:10.1016/j.conbuildmat.2023.134267
24. An H, Wang L, Lv F, Fu R, Lu Y, Kong D. Multi-objective optimization of properties on polymer fiber-reinforced desulfurization gypsum-based composite cementitious materials. *Constr. Build. Mater.* **2023**, *369*, 130590. DOI:10.1016/j.conbuildmat.2023.130590
25. Das AK, Leung CKY, Barbhuiya S. Experimental investigation and machine learning-based modelling of shrinkage evolution due to natural sea sand on fiber reinforced cementitious composites. *J. Sustain. Cem.-Based Mater.* **2025**, *14*, 2145–2165. DOI:10.1080/21650373.2025.2524763
26. Das AK, Xiao J. Upcycling waste glass bottles as a binder within engineered cementitious composites (ECCs): Experimental investigation and environmental impact assessment. *Clean. Mater.* **2025**, *16*, 100311. DOI:10.1016/j.clema.2025.100311
27. Ogirigbo OR, Black L. Influence of slag composition and temperature on the hydration and microstructure of slag blended cements. *Constr. Build. Mater.* **2016**, *126*, 496–507. DOI:10.1016/j.conbuildmat.2016.09.057
28. Zheng W, Dong J, Wen J, Chang C, Li Y, Wang Q. Effect of desulphurization gypsum on hardening mechanism of the geopolymer produced with steel slag and granulated blast furnace slag. *J. Mater. Cycles Waste Manag.* **2025**, *27*, 159–169. DOI:10.1007/s10163-024-02099-y
29. Zhou Y, Xie L, Kong D, Peng D, Zheng T. Research on optimizing performance of desulfurization-gypsum-based composite cementitious materials based on response surface method. *Constr. Build. Mater.* **2022**, *341*, 127874. DOI:10.1016/j.conbuildmat.2022.127874
30. Aziz A, Stocker O, El Amrani El Hassani I-E, Laborier AP, Jacotot E, El Khadiri A, et al. Effect of blast-furnace slag on physicochemical properties of pozzolan-based geopolymers. *Mater. Chem. Phys.* **2021**, *258*, 123880. DOI:10.1016/j.matchemphys.2020.123880
31. Lee B, Kim G, Nam J, Lee K, Kim G, Lee S, et al. Influence of α-Calcium Sulfate Hemihydrate on Setting, Compressive Strength, and Shrinkage Strain of Cement Mortar. *Materials* **2019**, *12*, 163. DOI:10.3390/ma12010163

32. Poupelloz E, Gauffinet S, Nonat A. Study of nucleation and growth processes of ettringite in diluted conditions. *Cem. Concr. Res.* **2020**, *127*, 105915. DOI:10.1016/j.cemconres.2019.105915
33. Sevim O, Sengul CG. Comparison of the Influence of Silica-rich Supplementary Cementitious Materials on Cement Mortar Composites: Mechanical and Microstructural Assessment. *Silicon* **2021**, *13*, 1675–1690. DOI:10.1007/s12633-021-01013-7
34. Liu L, Tan J, Qiu H, Zhang J, Guo Y. Study on microstructural and mechanical properties of cementitious materials composed of fly ash and dacite powder. *Front Mater* **2024**, *11*, 1267197. DOI:10.3389/fmats.2024.1267197